

Capturing the residence time boundary layer - Application to the Scheldt Estuary.

Sébastien Blaise · Benjamin de Brye
Anouk de Brauwere · Eric Deleersnijder
Eric J.M. Delhez · Richard Comblen

Ocean Dynamics, Volume 60, Number 3, June 2010
The final publication is available at www.springerlink.com

Abstract At high Peclet number, the residence time exhibits a boundary layer adjacent to incoming open boundaries. In a Eulerian model, not resolving this boundary layer can generate spurious oscillations that can propagate into the area of interest. However, resolving this boundary layer would require an unacceptably high spatial resolution. Therefore, alternative methods are needed in which no grid refinement is required to capture the key aspects of the physics of the residence time boundary layer. An X-FEM representation and a boundary layer parameterisation are presented and tested herein. It is also explained how to preserve local consistency in reversed time simulations so as to avoid the generation of spurious residence time extrema. Finally, the boundary layer parameterisation is applied to the computation of the residence time in the Scheldt Estuary (Belgium/The Netherlands). This timescale is simulated by means of a depth-integrated, finite element, unstructured mesh model, with a high space-time resolution. It is seen that the residence time temporal variations are mainly affected by the semidiurnal tides. However, the spring-neap variability also impacts the residence time, particularly in the sandbank and shallow areas. Seasonal variability is also observed, which is induced by the fluctuations over the year of the upstream flows. In general, the residence time is an increasing function of the distance to the mouth of the estuary. However, smaller-scale fluctuations are also present: they are caused by local bathymetric features and their impact on the hydrodynamics.

S. Blaise · B. de Brye · A. de Brauwere · E. Deleersnijder · R. Comblen
Université catholique de Louvain,
Center for Systems Engineering and Applied Mechanics (CESAME),
Avenue Georges Lemaitre, 4, B-1348 Louvain-la-Neuve, Belgium
E-mail: sebastien.blaise@uclouvain.be

A. de Brauwere
Vrije Universiteit Brussel,
Analytical and Environmental Chemistry,
Pleinlaan 2, B-1050 Brussels, Belgium

E. J.M. Delhez
Université de Liège,
MARE, Modélisation et Méthodes Mathématiques,
Sart Tilman B37, B-4000 Liège, Belgium

Keywords Residence time · Boundary layer · Parameterisation · X-FEM · Finite elements · Diagnostic · Adjoint modelling · Local Consistency

1 Introduction

The output files of most marine models are so huge that interpreting them is far from trivial, calling for the design and implementation of simple estimators of the state of the system under consideration (e.g. Deleersnijder and Delhez 2007). Several efforts have been made to introduce such estimators; among them it is worth mentioning timescales such as the age, flushing time, exposure time and residence time (Deleersnijder et al. 2001; Monsen et al. 2002; Delhez et al. 2004a,b; Delhez and Deleersnijder 2006; Delhez 2006). The latter is the time taken by a particle of water to touch an open boundary of a control domain for the first time (Bolin and Rhode 1973; Zimmerman 1976; Takeoka 1984; Delhez and Deleersnijder 2006). The exposure time is an analogous concept, defined to be the accumulated time during which water parcels stay in a control domain (Delhez 2006). Both diagnostics can be used; and the choice of the method depends on the context. The present study focuses on the residence time.

The definition of the residence time suggests a Lagrangian representation (Tartinville et al. 1997; Luther and Haitjema 1998; Meyers and Luther 2008). Then, random walks are necessary to represent diffusive processes (Nauman 1981; Allen 1982). The stochastic nature of Lagrangian approaches requires the computation of statistical quantities which are relevant only if the number of particles is large (e.g. Tartinville et al. 1997; Spivakovskaya et al. 2007). The direct Eulerian computation of the residence time is also possible (Wang et al. 2004; Soetaert and Herman 1995; Gourgue et al. 2007; Arega et al. 2008; Liu et al. 2008b). However, a specific tracer model run is required for the computation of the residence time at each location and at each time where and when the information is sought. Therefore, many tracer runs may be needed to estimate the residence time with a significant time-space resolution. The computing cost can be reduced by having recourse to the adjoint method recently developed by Delhez et al. (2004b). The latter allows one to obtain the residence time at any time and location in the whole domain by resolving an adjoint advection-diffusion problem in a backward time integration mode.

At high Peclet number, the residence time exhibits a boundary layer adjacent to incoming boundaries (Delhez and Deleersnijder 2006). This boundary layer, induced by the homogeneous Dirichlet condition imposed at open boundaries, makes the residence time difficult to compute with common numerical methods. In a Eulerian model, spurious oscillations are likely to be generated at incoming boundaries. These oscillations can propagate into the area of interest and affect the entire domain, leading to a non-physical residence time field. This issue does not occur when the exposure time is computed, as we do not prescribe boundary conditions at the boundary of the control domain.

Although the description of the boundary layer itself may not be that important for the interpretation of the results, its effect on the neighbouring field must be taken into account. Refining the grid so as to resolve the steep gradient of the residence time can overcome this issue, but the needed resolution would lead to an unacceptably large computing time. In this study, we present solutions to treat the boundary layer without increasing significantly the computing cost. They should help the modeller in computing the residence time distribution in any domain without any critical issue.

A first possible solution is based on X-FEM, the extended finite element method (Moës et al. 1999). X-FEM consists of a classical finite element method enriched by a set of test and shape functions especially designed to represent the solution whose analytical behaviour is known a priori. The method can represent exactly a solution that is known up to a multiplicative factor. The classical polynomial test and shape functions allow for a good approximation of the solution when it differs from the assumed behaviour (Hanert et al. 2007). Initially designed for fracture mechanics (Moës et al. 1999; Combescure et al. 2005; Wyart et al. 2008), this method was successfully applied to marine simulations for the representation of the logarithmic bottom boundary layer (Hanert et al. 2007).

The second method consists in parameterising the boundary layer. The latter is not explicitly resolved but appropriate boundary conditions, derived from the analytical solution of an idealised problem, are enforced. This kind of approach is also often used to treat the logarithmic bottom boundary layer. In this case, the bottom stress (i.e. the momentum flux) is parameterised as a quadratic function of the velocity, a formulation that is in agreement with the logarithmic nature of the velocity profile (Blumberg and Mellor 1987; Black and Gay 1987; Burchard 2002).

The present article is organized as follows. Section 2 introduces the adjoint method for a depth-integrated model, along with the boundary conditions to enforce. The issue of the boundary layer of the residence time is introduced in Section 3. Two solutions to handle this boundary layer, one derived from the extended finite element method and a parameterisation are developed and validated by means of a one-dimensional test case. Section 4 introduces the concept of local consistency and explains how to ensure it for multidimensional tracer simulations backward in time. In Section 5, the residence time is computed in a realistic problem, the flow in the Scheldt Estuary. Finally, conclusions are drawn in Section 6.

2 Residence time

The two-dimensional time-dependent residence time θ can be obtained by solving backward in time the partial differential equation

$$\frac{\partial(H\theta)}{\partial t} + \nabla \cdot (H\mathbf{u}\theta) = \nabla \cdot [(-\kappa)H\nabla\theta] - H, \quad (1)$$

where t is the time, while \mathbf{u} , κ and H denote the depth-averaged horizontal velocity, the diffusivity and the total water depth, which is the sum of the surface elevation (positive upwards) and the reference water depth. It must be stressed that this equation is not a classical depth-integrated advection-diffusion equation (with a production term). If it were so, the diffusivity term would appear with a positive sign in the right-hand side, while it is negative here. In fact, equation (4) is obtained from an adjoint approach similar to that of Delhez et al. (2004b). Details of its derivation may be found in Appendix A.

Equation (4) must be integrated backward in time, otherwise the differential problem dealt with would be ill-posed (e.g. Garabedian 1964). The physical meaning of this backward integration is that the residence time at time t depends on the dynamics within the interval $[t, \infty]$. The backward integration starts at time T , which corresponds to the end of the physical simulation time (i.e. the beginning of the reverse integration time). Introducing $\tau = T - t$, equation (4) transforms to

$$\frac{\partial(H\theta)}{\partial\tau} + \nabla \cdot [H(-\mathbf{u})\theta] = \nabla \cdot (\kappa H \nabla \theta) + H, \quad (2)$$

which is a classical tracer equation with reversed velocity and a source term.

The residence time is the time taken by a water parcel to touch an open boundary of a control domain for the first time. Water parcels can flow out of the control domain through open boundaries, but they are completely ignored from the moment they leave the domain. A homogeneous Dirichlet boundary condition must be enforced at open boundaries to ensure that the water parcels touching the boundary are removed from the computation (Delhez et al. 2004b; Delhez and Deleersnijder 2006). In addition, a no-flux condition is imposed at closed boundaries (Delhez et al. 2004b):

$$\theta = 0 \quad \text{at open boundaries,} \quad (3)$$

$$\mathbf{n} \cdot (H \nabla \theta) = 0 \quad \text{at closed boundaries,} \quad (4)$$

where \mathbf{n} is the outgoing unit normal to the boundary. Unfortunately, at high Peclet number, condition (3) induces a boundary layer in the vicinity of the open boundary where the flow is into the control volume. This boundary layer must be treated in a suitable manner in order to prevent spurious oscillations from developing.

3 One-dimensional developments

To gain insight into the residence time boundary layer issue, consider first a one-dimensional steady-state configuration with a constant depth. The domain is defined by $0 \leq x \leq L$ where x is the spatial coordinate. For simplicity, the velocity $u = U$ and the diffusivity $\kappa = K$ are taken to be positive constants. This configuration can be interpreted as a highly idealised channel (Delhez et al. 2004b). Under these assumptions, equation (2) simplifies to

$$K \frac{d^2\theta}{dx^2} + U \frac{d\theta}{dx} + 1 = 0. \quad (5)$$

The boundaries are assumed to be open. Therefore, according to condition (3), the residence time is prescribed to be zero at $x = 0$ and $x = L$. This equation can be adimensionalised, using $x = \tilde{x}L$ and $\theta = \tilde{\theta}L/U$, and defining the Peclet number Pe as UL/K . This yields

$$\frac{1}{Pe} \frac{d^2\tilde{\theta}}{d\tilde{x}^2} + \frac{d\tilde{\theta}}{d\tilde{x}} + 1 = 0. \quad (6)$$

For the sake of simplicity, the tildes are dropped hereinafter.

Solving equation (6) under the abovementioned Dirichlet boundary conditions leads to

$$\theta(x) = \frac{1 - e^{-Pe x}}{1 - e^{-Pe}} - x. \quad (7)$$

As pointed out by Delhez and Deleersnijder (2006), this solution exhibits a boundary layer near the inflow boundary, i.e. in the vicinity of $x = 0$. The thickness of this boundary layer is of the order of Pe^{-1} , i.e. K/U in dimensional variables. This can be seen in Figure 1 for values of the Peclet number ranging from 10 to 1600. Figure 1

also shows the results of a linear finite-element resolution of equation (5), with a mesh made up of ten elements. Accordingly, the solution is approximated by

$$\theta(x) \approx \theta_{\text{fem}}^h = \sum_{j=1}^N \theta_j \phi_j(x), \quad (8)$$

where ϕ_j is a piecewise linear shape function corresponding to the j -th node of the mesh whose total number of nodes is N . The nodal values associated with the shape functions ϕ_j are denoted θ_j . Figure 1 shows that the solution oscillates if the Peclet number is higher than a threshold value. Although generated by the inflow boundary condition, the oscillations affect the whole computational domain. The linear finite elements scheme used for the one-dimensional simulation with U and K constants and a uniform mesh is strictly equivalent to a finite-differences scheme. For that finite-differences scheme, it is shown in Appendix B that oscillations appear when the mesh Peclet number $Pe^h = U\Delta x/K$ is higher than 2, where Δx is the grid spacing. This is illustrated in Figure 1, which exhibits spurious oscillations for $Pe^h > 2$.

The numerical oscillations are generated by the discretisation of the advection term and the problem could be addressed by refined advection schemes, i.e. Total Variation Diminishing - TVD, Flux-Corrected Transport (Kuzmin et al. 2005), slope limiters (Cockburn and Shu 1998) or artificial viscosity (Arminjon and Dervieux 1993). Although such methods are relatively efficient and easy to implement in an explicit model, they can become intricate with an implicit time-discretisation such as used in this paper. They also involve a larger computational overhead. More basically, the amount of artificial diffusion introduced by these schemes can alter significantly the flux of residence time through the open boundary. The methods described in this paper involve no excessive numerical diffusion, even near the incoming open boundaries. The discontinuous Galerkin method is used, which is linear and has proven to be efficient and accurate for convection dominated flows. Thuburn and Haine (2001) showed that the computation of the adjoint of a non-linear advection scheme can lead to ambiguous results which do not reflect the physical behaviour of the system. Then, computing the adjoint of the forward problem with a non-oscillatory advection scheme that is better than first-order accurate (hence non-linear) cannot be done. Other techniques have to be considered to address the issue of the residence time boundary layer with an accurate discretisation.

One may have recourse to the X-FEM method (Moës et al. 1999), which is able to represent exactly a solution known up to a multiplicative factor. A polynomial component needs to be retained to take into account the discrepancies between the actual solution and that assumed in X-FEM. Details of the implementation of the method can be found in Appendix C. It produces results (Figure 2b) that do not show the strong oscillations that appear when a classical finite element method is used (Figure 1), and are very close to the analytical solution (Figure 2a). However, Appendix C describes some difficulties that could be an obstacle to its application in a realistic model. Because of these difficulties, it seems appropriate to look for another solution to deal with the boundary layer. An alternative consists in a parameterisation, derived from the analytical solution of the one-dimensional steady-state problem. The idea is to derive an appropriate boundary condition for the outer solution of the boundary layer problem (Figure 3). The representation of the boundary layer is indeed not crucial as long as its impact on the residence time in the interior of the computational domain is taken into account.

We need to enforce a correct boundary condition at the limit of the computational domain. The one-dimensional steady-state equation for the residence time (5) is an ordinary differential equation which can be solved analytically. We first assume that the velocity and diffusivity are constant in the parameterised zone. This hypothesis is acceptable, as this zone generally is very narrow compared with the other length scales of the flow under consideration. Furthermore, the boundary for the residence time is not a physical boundary for the hydrodynamics (i.e. it is just an arbitrary limit fixed by the user), and thus does not affect the velocity and diffusivity. Under these hypotheses, equation (5) will be solved in the parameterised domain to obtain the gradient to enforce (Neumann condition) at the boundary of the computational domain. Following condition (3), a zero residence time is to be imposed at $x = 0$, and we denote θ^* the value of the residence time computed by the model at $x = L^*/L$ (see Figure 3), the boundary of the computational domain (called hereafter numerical boundary). Then, the exact expression of the residence time may be rewritten as follows

$$\theta = \frac{e^{-Pe x} - 1}{e^{-Pe \frac{L^*}{L}} - 1} \left(\theta^* + \frac{L^*}{L} \right) - x. \quad (9)$$

To know the gradient to impose at the numerical boundary, expression (9) is differentiated with respect to x and then evaluated at $x = L^*/L$, leading to

$$\left. \frac{d\theta}{dx} \right|_{x=\frac{L^*}{L}} = Pe \frac{e^{-Pe \frac{L^*}{L}}}{1 - e^{-Pe \frac{L^*}{L}}} \left(\theta^* + \frac{L^*}{L} \right) - 1, \quad (10)$$

which corresponds in dimensional form to

$$\left. \frac{d\theta}{dx} \right|_{x=L^*} = \frac{1}{K} \frac{e^{-UL^*/K}}{1 - e^{-UL^*/K}} (\theta^*U + L^*) - \frac{1}{U}. \quad (11)$$

This technique provides numerical results that are devoid of any oscillation (Figure 2c) and very close to the analytical solution (Figure 2a). It must be stressed, however, that the presence of an oscillating mode is not directly related to the boundary conditions (3); this mode is part of the general solution of the discrete equation if the Peclet number exceeds a critical value (i.e. when $Pe^h > 2$). However, selecting the appropriate strategy to impose boundary conditions can strongly reduce the amplitude of the oscillatory mode, particularly at high Peclet number (Appendix D).

As the X-FEM and parameterisation methods were developed from a time-independent analytical solution, it is useful to validate them on a transient simulation to make sure that they are still relevant if the solution varies in time. In a time-dependent configuration, the velocity in the parameterised region, U , can sometimes be equal to zero. If so, (10) contains divisions by zero, and cannot be computed. This case must be treated separately. If $U = 0$, the advection term of equation (5) vanishes, and the equation for the residence time reduces to

$$K \frac{d^2\theta}{dx^2} = -1. \quad (12)$$

Under the previously-used assumptions, the analytical solution of equation (12) in the parameterised zone is

$$\theta = -\frac{x^2}{2K} + \frac{L^*x}{2K} + \frac{\theta^*x}{L^*}. \quad (13)$$

Therefore, the gradient to enforce on the numerical boundary is

$$\frac{d\theta}{dx} = -\frac{x}{K} + \frac{L^*}{2K} + \frac{\theta^*}{L^*}. \quad (14)$$

Expressions (10) and (14) exhibits terms that are linear in θ^* , the other terms being independent of θ^* . The former terms must be treated implicitly to ensure the stability of the numerical method. Due to the stiffness of the problem, an unacceptably small explicit time step would be needed to capture the relevant time-scales.

To validate the method for a time-dependent flow, we consider the same one-dimensional domain, the velocity U being modulated in time by a sine representing an idealised tide. A residual velocity $U_{\text{residual}} = U_{\text{tide}}/100$ is considered, where U_{tide} is the amplitude of the velocity associated with the tidal oscillations. The variables are still dimensionless, and the ratios between parameters are chosen to be comparable to a realistic situation, roughly similar to the characteristic scales encountered in the simulations of the Scheldt Estuary (Section 5). The tidal period is $T_{\text{tide}} = 0.864$. The Peclet number is set to $Pe = 1000$. The left half of the domain has a mesh size of $0.02L$, leading to a maximum mesh Peclet number $Pe^h = 20$. The right half of the domain has a mesh resolution of $10^{-3}L$. Only the left open boundary is treated specifically, while the right open boundary has a sufficient resolution to handle the boundary layer. An implicit Euler time-stepping scheme is employed, and the time-discretisation of the one-dimensional idealised equation reads

$$\frac{\theta^{n+1} - \theta^n}{\Delta\tau} = K \frac{\partial^2 \theta^{n+1}}{\partial x^2} + U \frac{\partial \theta^{n+1}}{\partial x} + 1. \quad (15)$$

A first run is performed using a high-resolution model (mesh size of $10^{-3}L$) so as to obtain a reference solution (Figure 4a). To remove the effects of initialisation, the solution is shown after a simulation time of 30 tidal periods, corresponding approximately to twice the residence time (Delhez et al. 2004b). Due to the residual flow, the peak of the residence time is shifted towards the left of the domain; and the solution is asymmetric. This is clearly visible in the middle of the domain, represented by the dashed lines on Figure 4. The X-FEM solution (Figure 4b) is very good and cannot be distinguished from the high-resolution solution, even in the boundary layer. The parameterised solution (Figure 4c) does not show the boundary layer (the blank space in Figure 4c correspond to the boundary layer where no solution is available). In the rest of the domain, the residence time is well computed and the results are similar to the reference solution (Figure 4a).

While the X-FEM method allows for an excellent representation of the boundary layer, it was pointed out above that its application in a two-dimensional realistic model can become quite intricate. For this reason, and as we do not need to know exactly the shape of the boundary layer, we will only use the parameterisation method for the realistic application. This method has the advantage of being very simple to implement.

4 Solving the equation backward in time

Integrating backward in time is particularly difficult when dealing with parabolic equations. The ill-posedness of the backward problem requires the use of adequate methods to ensure a continuous dependence on the final data (Payne 1975; Elden 1982; Liu et al. 2008a). The backward in time integration of the residence time equation is a well-posed

problem, as the diffusivity coefficient is negative. It can be solved like a classical forward advection-diffusion equation. However, as for any simulation involving hydrodynamics and tracer simulations, special attention must be paid to local consistency.

A passive tracer simulation is said to be locally consistent if the numerical scheme is such that the tracer concentration remains constant as time progresses, assuming that the initial concentration was homogeneous in space (White et al. 2008). This concept may be applied to the transport terms of the residence time equation, in order to prevent the development of spurious extrema. The latter can be rather strong in coastal and estuarine areas, partly because the sea surface elevation is in many locations of the same order of magnitude as the unperturbed depth. White et al. (2008) showed that a discrete compatibility between the free-surface equation

$$\frac{\partial H}{\partial t} + \nabla \cdot (H\mathbf{u}) = 0 \quad (16)$$

and the tracer equation must be fulfilled to ensure consistency. This compatibility is of two kinds:

- **Spatial compatibility** is ensured if the discrete advection operator for a unit tracer simplifies to the divergence term of the free-surface equation $\nabla \cdot (H\mathbf{u})$. This is obtained by using the same element to represent sea surface elevation and tracers. Here we use linear discontinuous Galerkin elements: the fields are represented using linear shape functions, and some discontinuities are allowed between elements. This method requires the computation of fluxes at the interfaces between elements. Due to their discontinuous representation, the variables needed to compute those fluxes are not uniquely defined and a Riemann solver is used to obtain a unique value that guarantees a stable and accurate formulation (Comblen et al. 2009). To ensure consistency, the Riemann solver used to deduce interface values for velocities and sea-surface elevation must be the same for tracer and continuity equations. The mesh used to compute the residence time is a submesh of the global mesh used for the hydrodynamics simulations. Hence, there is no error due to interpolation or projection of data.
- **Temporal compatibility** is more complex, as we use a residence time simulation which is reversed in time. As we use an implicit Euler method, the time discretisation of the free surface equation (16) reads

$$\frac{H^{n+1} - H^n}{\Delta t} = -\nabla \cdot (H^{n+1}\mathbf{u}^{n+1}), \quad (17)$$

The superscripts correspond to the time step at which the variables are expressed, $n + 1$ being the new time step in the physical time (forward simulation) and n being the old one. If we reverse the time of the simulation, $n + 1$ and n need to be switched in the mass term. The opposite of the velocity must be taken for the divergence term, the latter still being computed at time $n + 1$ to be consistent with the forward simulation:

$$\frac{H^n - H^{n+1}}{\Delta \tau} = -\nabla \cdot (H^{n+1}(-\mathbf{u}^{n+1})). \quad (18)$$

The variables used for the residence time equation (2) must be taken at the same time as the corresponding variables in the free surface equation. Thus, the time discretisation of the residence time equation (2) reads

$$\frac{H^n \theta^n - H^{n+1} \theta^{n+1}}{\Delta \tau} = -\nabla \cdot (H^{n+1}(-\mathbf{u}^{n+1})\theta^n). \quad (19)$$

Only the advection and mass terms are taken into account as they are the only ones that need to be compatible with the free surface equation. Source and diffusion terms do not break consistency because the first one is constant over the whole domain and the second one depends on the gradient of the residence time concentration, which is zero if the tracer is constant in space. It is obvious that, for a constant θ , expressions (18) and (19) are equivalent. We thus need to use the variables H and \mathbf{u} at the times corresponding to equation (19) to ensure the local consistency when time is reversed. Hydrodynamic results must then be saved at each time step to reload them for the adjoint simulation. Thanks to the implicit time-stepping scheme, a relatively large time step can be used, and the disk space required to store the results of the forward simulation is not excessive (e.g. the two-year simulation with a time step of 10 minutes described in section 5 required 47 Gb to store the state of the hydrodynamic variables at each time step).

For larger problems, a checkpointing mechanism can be used to reduce the disk storage requirements, at the expense of additional recomputations (Alexe and Sandu 2009). During the forward simulation, the state of the hydrodynamic variables is stored only at some specific time steps, called checkpoints. For the backward simulation, the checkpoints are read in the reverse order, and the variables at each time step between two checkpoints must be recomputed using the forward model. If the number of time steps between two checkpoints is not too large, the state of the hydrodynamic variables between two checkpoints can be stored in the working memory. Another technique to reduce the storage requirements is to store the data at some specific time steps and interpolate the variables between those saved time steps. However, the temporal accuracy of the results will be altered. Furthermore, the interpolation scheme should be chosen with care to maintain conservation and consistency (Deleersnijder 1993).

5 Application to a two-dimensional realistic problem

The residence time is now computed in a two-dimensional realistic domain, i.e. the Scheldt Estuary (Belgium/The Netherlands). First, the hydrodynamics is simulated using the two-dimensional version of the finite element model SLIM (Comblen et al. 2009; de Brye et al. 2009, <http://www.climate.be/SLIM>). This hydrodynamic simulation concerns most of the North Western European Continental Shelf, the Scheldt Estuary, the Scheldt River and the fraction of its tributaries under the influence of tides, the latter two being represented by one-dimensional elements (Figure 5). The residence time is then computed backward in time in the Scheldt Estuary sub-domain. The computational grid is unstructured and refined in the regions of interest (e.g. the Scheldt Estuary) or where the dynamics is more demanding (e.g. next to coastlines). The mesh is made up of 26000 triangular elements, and 5000 of them are located in the Scheldt Estuary. The river and its tributaries are represented by 350 line elements. The mesh size is about 400 m in the one-dimensional river and tributaries; and it varies from 150 metres to 30 kilometres in the two-dimensional domain. The minimum thickness of the boundary layer $\frac{\kappa}{(-\mathbf{n}\cdot\mathbf{u})_{\max}}$ is approximately 10 metres near the upstream boundary and 70 metres near the sea mouth boundary. The characteristic spatial resolution at the estuary/river interface (150 m) and at the sea mouth (400 m) provides the reference value for the length scale L^* used in the boundary representation. The model and its validation on the present domain are described in detail by de Brye

et al. (2009). At the shelf break, the sea surface elevation is prescribed from values of the TPXO model, which assimilates satellite altimetry data (Egbert et al. 1994). The following tidal constituents are taken into account: M_m , M_f , Q_1 , O_1 , P_1 , K_1 , N_2 , M_2 , S_2 , K_2 , and M_4 . The surface atmospheric pressure and the wind velocity are obtained from the NCEP Reanalysis data provided by the NOAA/OAR/ESRL PSD (Kalnay et al. 1996). The non-tidal part of the flow in the Scheldt and its tributaries is obtained from various sources, which are mentioned in de Brye et al. (2009).

Figure 6 shows the evolution of the residence time in the Scheldt Estuary on February 1, 2001. As the residence time is defined to be the time needed to touch an open boundary of the estuary for the first time, the residence time decreases towards both the upstream and downstream ends. Obviously, most of the water will eventually leave through the mouth of the estuary, because the residual current is directed from the land to the sea. However, due to the tidal motion, some water can indeed cross the upstream boundary first. The residence time varies with the tidal phase. At the sea mouth, the residence time is highest at the end of the ebb tide, because the water will be pushed into the estuary during the coming rising water. Conversely, at the end of flood tide, the residence time is relatively low. This simply reflects the fact that external water has been entering the estuary during rising tide but much of it will be pushed back out soon. The opposite behaviour is observed at the upstream boundary, where rising water correspond to an outflow: the residence time is highest at the end of flood tide, while it is lowest at the end of ebb tide. In addition to tidal effects, Figure 6 also shows that the residence time varies spatially, due to bathymetry and related hydrodynamical features. For instance, the large tidal flat area of the Verdrongen Land van Saeftinghe (Figure 6a), is associated with longer residence times than the surroundings. This is because this area is very shallow with a few trenches (the only parts included in the computational domain) and therefore the water velocity is rather low. It is the first time residence times in the Scheldt Estuary have been estimated in such a detailed way, i.e. with such a space-time resolution. The range of the residence time (0 - 56 days) corresponds well with previous studies estimating residence times in a number of longitudinal boxes (0 - 50 days, Soetaert and Herman (1995)) or the nominal flushing time for the entire estuary (25 - 65 days, Steen et al. (2002)). Note that these results refer to winter situations and that the residence time tends to increase significantly in summer, up to 70 days (Soetaert and Herman 1995) or even higher, depending on how much the freshwater discharge decreases. This seasonal variation, related to the Scheldt flow variability, is also observed in Figure 7 showing the mean residence time over the whole estuary, as it is computed backward from December 31 to January 1, 2001. Besides the seasonal cycle and the high frequency variability of the semi-diurnal tidal cycle (discussed above), Figure 7 also displays a fortnightly variation in the mean residence time, corresponding to the spring-neap tidal cycle. Note that the results from November, 2001 to December, 2001 correspond to the initialisation of the backward simulations and cannot be trusted. According to Delhez et al. (2004b), the results become significant after an initialisation period whose duration is about twice the mean residence time, i.e. about two months.

It is interesting to understand how different tidal components act upon the residence time. To this aim, a tidal decomposition using the **T-TIDE** software (Pawlowicz et al. 2002) was performed on the residence time field with data covering the period from May, 2001 to October, 2001. Figure 8 shows the amplitudes of the residence time fluctuations associated with the M_2 , S_2 and M_{sf} tidal components. As the adjoint method is used to compute the residence time, these amplitudes can be computed over

the whole domain. As in the hydrodynamics, the M_2 component is clearly dominant. This variability is related to the displacement of the residence time structure by the tidal excursion. The S_2 signal is weaker, but its amplitude distribution over the domain is very similar. This is due to the fact that semi-diurnal lunar (M_2) and solar (S_2) components are characterised by a similar period (respectively 12.42 h and 12 h). The small amplitudes next to the boundaries are an effect of the boundary layer related to the fact that the residence time should be zero at the open boundaries. However, the variability a few kilometers downstream the upstream boundary is very high. The water at rising tide will be carried to the river and will then leave quickly the control domain. At falling tide, most of the water in this zone will flow toward the sea mouth and after many tidal cycles will exit the control domain by the downstream boundary. Its residence time will then be much higher, explaining the high variability in this region. The fortnightly signal M_{sf} of period 13.66 days is induced by the combination of M_2 and S_2 components. As this signal is related to slower variations, it generates a larger boundary layer compared to semi-diurnal components. The residence time in the trenches of the Verdrongen Land van Saeftinghe is almost not affected by tidal components, because the temporal variability of the residence time is limited in this zone. However, a slight temporal variation is related to the M_{sf} period. This is because the variations associated with the main flow are too fast to significantly influence the residence time in this zone; but the variations of the flow corresponding to the fortnightly tidal component are slow enough to drain or fill sufficiently the trenches to impact somewhat the residence time. The residence time variations associated with the fortnightly signal are stronger on sandbanks, because these areas have a relatively large water depth during spring tides (lower residence time), but are covered with a thin layer of water during neap tides, enhancing the relative impact of bottom friction (higher residence time).

Figure 9 shows the residence time along a longitudinal section from the estuary/river interface. The snapshots are taken at times similar to those of Figure 6. As expected, the residence time remains always positive, and tends to zero at the boundaries. The influence of the boundary layer is visible at 11h00. After that time, the water flux enters in the estuary from the river. This inflow boundary influences the residence time in the backward simulations to create the boundary layer which is fully developed at 11h00. For the solution using the parameterisation of the boundary layer, the latter is entirely comprised in the parameterised zone, while the solution using a Dirichlet boundary condition oscillates. If we continue back in time, the outgoing flux breaks the boundary layer and the residence time decreases smoothly in space near the boundary. The residence time at both inflows and outflows is well represented by the model. In the case of the Scheldt Estuary, the issue of the boundary layer is rendered less severe by the time dependency of the flow, as the boundary layer disappears every time the tide reverses. In a flow exhibiting a unique direction, this problem would be more critical as the boundary layer would be present during the whole simulation (Delhez and Deleersnijder 2006).

6 Conclusion

The adjoint method from Delhez et al. (2004b) presumably is the only one that allows one to obtain at an acceptable CPU cost the residence time at any time and location in the domain of interest. Thus, the residence time is also computed near boundaries,

where it exhibits a boundary layer whose characteristic length is generally much smaller than the mesh size.

Two methods were presented for dealing with the residence time boundary layer without explicitly resolving it. The first one, using the extended finite elements method, consists in enriching the functional space available for the representation of the field with shape functions derived from an idealised analytical solution. It is able to represent the boundary layer itself with a high degree of precision and has been validated on one-dimensional stationary and non-stationary configurations. While this method seems promising to represent the boundary layer of the residence time, its implementation in a two-dimensional or three-dimensional realistic model is likely to present insuperable difficulties.

The second method is a parameterisation of the boundary layer, in which the latter is not explicitly resolved. The effect of the boundary layer is parameterised by imposing on the boundary a normal gradient of the solution, whose expression was developed from an idealised analytical solution. This method is easy to implement in realistic models and produces results which are physically acceptable and devoid of any spurious oscillation. It was validated on both one-dimensional and two-dimensional simulations.

The residence time was computed in the Scheldt Estuary with a high level of detail. The amplitudes of its variations associated with the main tidal components were obtained over the whole domain, showing that the residence time temporal variability is mainly affected by the semidiurnal signals. However, the spring-neap variability also has an influence on the residence time, particularly in the sandbanks and shallow areas. On top of the tidal effects, the residence time varies spatially, due to the bathymetry and related hydrodynamical processes.

The use of the adjoint method to compute the residence time addresses the problem of spatial and temporal consistency, which are mandatory to obtain acceptable results. The way to preserve consistency, specifically for reversed time simulation, was explained in detail.

For computing the residence time, the adjoint method has strong advantages over other methods, such as forward Lagrangian approaches or forward Eulerian models. It should help significantly doing physical diagnoses. However, its implementation is more complex due to the integration backward in time and the boundary layer treatment. This article is a complement to Delhez et al. (2004b) and should help the modeller in computing the residence time distribution in any domain without any critical issue.

Acknowledgements Sébastien Blaise is a Research fellow with the Belgian Fund for Research in Industry and Agriculture (FRIA). Richard Comblen and Eric Deleersnijder are respectively Research fellow and Research associate with the Belgian National Fund for Scientific Research (FNRS). Eric Delhez is honorary Research Associate with the Belgian National Fund for Scientific Research. Anouk de Brauwere is a postdoctoral researcher at the Research Foundation Flanders (FWO-Vlaanderen). The present study was carried out within the scope of the project “A second-generation model of the ocean system”, which is funded by the *Communauté Française de Belgique*, as *Actions de Recherche Concertées*, under contract ARC 04/09-316, and the project “Tracing and Integrated Modelling of Natural and Anthropogenic Effects on Hydrosystems” (TIMOTHY), an *Interuniversity Attraction Pole* (IAP6.13) funded by the *Belgian Federal Science Policy Office* (BELSPO). This work is a contribution to the development of SLIM, the Second-generation Louvain-la-Neuve Ice-ocean Model (<http://www.climate.be/SLIM>). The authors are indebted to Emmanuel Hanert and Olivier Gourgue for their useful comments.

A Derivation of the two-dimensional residence time equation

The equation (4) for the depth-averaged residence time can be derived by adapting the procedure introduced in Delhez et al. (2004b) in the context of a three-dimensional model.

In the context of two-dimensional depth-integrated model, the (mean) residence time in a control domain ω at a particular location \mathbf{x}_0 and a given time t_0 is given by

$$\theta(t_0, \mathbf{x}_0) = \int_{t_0}^{\infty} \left(\iint_{\omega} H(t, \mathbf{x}) C(t, \mathbf{x}) d\mathbf{x} \right) dt \quad (20)$$

where $C(t, \mathbf{x})$ denotes the concentration field produced by a unit point discharge at \mathbf{x}_0 at time t_0 and where H is the total water depth (which is the sum of the surface elevation and the reference water depth).

In a direct approach, C is obtained by solving the advection-diffusion problem

$$\begin{cases} \frac{\partial(HC)}{\partial t} + \nabla \cdot (H\mathbf{u}C) = \nabla \cdot (\kappa H \nabla C) \\ H(t_0, \mathbf{x}) C(t_0, \mathbf{x}) = \delta(\mathbf{x} - \mathbf{x}_0) \\ C = 0 & \text{at the open boundaries of } \omega, \\ \mathbf{n} \cdot \kappa H \nabla C = 0 & \text{at material boundaries of } \omega, \end{cases} \quad (21)$$

where \mathbf{u} and κ denote respectively the depth-averaged horizontal velocity and the diffusivity and where δ is the Dirac impulse function. Using this approach, the direct problem (21) must be solved for a variety of initial conditions corresponding to the times and locations at which the residence time is sought, which can be very demanding in computer resources.

An alternative and more efficient procedure can be derived by considering the adjoint of (21). To this end, we define the adjoint variable C_T^* as the solution of the differential problem

$$\begin{cases} H \frac{\partial C_T^*}{\partial t} + H\mathbf{u} \cdot \nabla C_T^* + \nabla \cdot (\kappa H \nabla C_T^*) = 0 \\ C_T^*(T, \mathbf{x}) = 1 & \text{in } \omega, \\ C_T^* = 0 & \text{at the open boundaries of } \omega, \\ \mathbf{n} \cdot \kappa H \nabla C_T^* = 0 & \text{at material boundaries of } \omega. \end{cases} \quad (22)$$

where T denotes some fixed time horizon.

Using (21) and (22), it is easy to show that (see Delhez et al. 2004b)

$$C_T^*(t_0, \mathbf{x}_0) = \iint_{\omega} H(T, \mathbf{x}) C(T, \mathbf{x}) d\mathbf{x} \quad (23)$$

so that the adjoint variable can be interpreted as the amount of the tracer considered in the direct problem that is still present in the control domain at time T , *i.e.* the fraction of the mass of the tracer released at time t_0 and location \mathbf{x}_0 with a residence time larger than $T - t_0$. One has therefore

$$\theta(t_0, \mathbf{x}_0) = \int_{t_0}^{\infty} C_t^*(t_0, \mathbf{x}_0) dt = \int_0^{\infty} D(t_0, \tau, \mathbf{x}_0) d\tau \quad (24)$$

where we introduced the cumulative distribution function

$$D(t_0, \tau, \mathbf{x}_0) = C_{t_0+\tau}^*(t_0, \mathbf{x}_0) \quad (25)$$

With this definition and using the depth-integrated continuity equation

$$\frac{\partial H}{\partial t} + \nabla \cdot (H\mathbf{u}) = 0 \quad (26)$$

it is easy to show from (22) that D satisfies the differential equation

$$\frac{\partial HD}{\partial t} - \frac{\partial HD}{\partial \tau} + \nabla \cdot (H\mathbf{u}D) + \nabla \cdot (\kappa H \nabla D) = 0 \quad (27)$$

and the auxiliary condition

$$D(t, 0, \mathbf{x}) = 1 \quad \text{in } \omega. \quad (28)$$

Integrating (27) with respect to τ and assuming that $D(t, \tau, \mathbf{x})$ decreases to zero when τ tends to infinity, *i.e.* that all the particles are eventually flushed out of the control domain, one gets finally

$$\frac{\partial H\theta}{\partial t} + H + \nabla \cdot (H\mathbf{u}\theta) + \nabla \cdot (\kappa H \nabla \theta) = 0 \quad (29)$$

which is the differential equation for the (mean) depth-averaged residence time in ω .

B Constraint on the mesh Peclet number

Starting from equation (6), we will solve the steady-state, one-dimensional problem defined in section 3 by means of a finite difference scheme.

The domain is discretised by N finite difference nodes of indices $n = 1 \rightarrow N$, whose locations are defined by $\tilde{x}_n = (n - 1/2)/N$. The grid resolution is then defined by $\Delta\tilde{x} = 1/N$. The discrete residence time at these points is noted $\tilde{\theta}_n^h$, where h refers to the approximate value of the variable. Two fictitious points are added beyond both boundaries of the domain (i.e. at $\tilde{x}_0 = -1/(2N)$ and $\tilde{x}_{N+1} = 1 + 1/(2N)$) whose values will be noted $\tilde{\theta}_0^h$ and $\tilde{\theta}_{N+1}^h$. These points will be useful to enforce the Dirichlet boundary conditions, as no grid point is defined on the boundary. The simplest centered finite-difference discretisation of the non-dimensional form of equation (6) yields

$$\frac{1}{Pe} \frac{\tilde{\theta}_{n+1}^h - 2\tilde{\theta}_n^h + \tilde{\theta}_{n-1}^h}{\Delta\tilde{x}^2} + \frac{\tilde{\theta}_{n+1}^h - \tilde{\theta}_{n-1}^h}{2\Delta\tilde{x}} + 1 = 0, \quad n = 1, 2 \dots N. \quad (30)$$

Boundary conditions, which consist in a zero residence time at each boundary, are enforced by imposing

$$\begin{aligned} \frac{\tilde{\theta}_0^h + \tilde{\theta}_1^h}{2} &= 0, \\ \frac{\tilde{\theta}_N^h + \tilde{\theta}_{N+1}^h}{2} &= 0. \end{aligned} \quad (31)$$

The solution of the discrete problem defined by (30) and (31) is of the form

$$\tilde{\theta}_n^h = Ar^n + Bn + C \quad (32)$$

where

$$r = \frac{2 - Pe\Delta\tilde{x}}{2 + Pe\Delta\tilde{x}}, \quad (33)$$

$$A = \frac{2}{(1+r)(r^N - 1)}, \quad (34)$$

$$B = -\frac{1}{N}, \quad (35)$$

$$C = \frac{1}{1 - r^N} + \frac{1}{2N}. \quad (36)$$

The constant r then satisfies

$$-1 < r < 1. \quad (37)$$

When the mesh Peclet number $Pe^h = Pe\Delta\tilde{x}$ is higher than 2, the constant r is negative, and a spurious oscillating mode appears in the solution (32). In dimensional variables, the critical factor Pe^h becomes $Pe\Delta x/L$. It can be written as $\Delta x/(LPe^{-1})$, i.e. the mesh size divided by the thickness of the boundary layer.

C X-FEM method for the one-dimensional problem

Using the X-FEM method, the set of shape functions in (8) is enriched with shape functions derived from the exact solution:

$$\theta(x) \approx \theta_{\text{fem}}^h + \theta_{\text{x-fem}}^h = \sum_{j=1}^N \theta_j \phi_j(x) + \sum_{j=1}^{N_x} b_j \phi_j(x) F(x), \quad (38)$$

where N_x is the number of enriched nodes. $F(x)$ is a function derived from the *a priori* known shape of the solution. It describes the solution up to a multiplicative factor that is to be determined. For the present one-dimensional experiment, this function is meant to represent the boundary layer. It is obtained by extracting from the exact solution (7) the part that is associated with the steep residence time gradient in the boundary layer, i.e.

$$F(x) = 1 - e^{-Pe x}. \quad (39)$$

The second term of (7) is linear and, hence, does not exhibit a boundary layer. It will then be handled by the classical linear shape functions. Thus, multiplying (39) by a nodal factor in combination with the linear shape functions contribution will allow for a good representation of the solution.

The residence time is computed in the idealised one-dimensional channel using X-FEM. The mesh is made up of 10 elements ($N = 11$) with an enriched shape function for the first node of the mesh, corresponding to the inflow boundary ($N_x = 1$). The X-FEM results (Figure 2b) do not show the strong oscillations that appear when a classical finite element method is used (Figure 1), and are very close to the analytical solution (Figure 2a). However, oscillations still appear for moderate mesh Peclet numbers (e.g. when $Pe^h = 5, 10, 20$). These oscillations appear only when the first node is enriched and the boundary layer length exceeds the width of the enrichment zone. One might think that it is desirable to enrich more nodes. But, when doing so, problems arise, especially if extended shape functions are present where the solution is quasi-linear. In this case, the enriching function $F(x)$ is almost equal to 1, and the linear system to be solved becomes ill-conditioned because $\phi_j(x)$ and $\phi_j(x)F(x)$ are almost equivalent. It is thus safe to enrich only the node that is adjacent to the boundary, or to resort to a strategy consisting in determining *a priori* the number of nodes to enrich to obtain the most accurate solution while retaining a well-conditioned system. The second option is unlikely to be easy to implement. Furthermore, in many realistic applications, the width of the boundary layer is generally much smaller than the element size, implying that enriching only the first node will be sufficient in most cases.

While the X-FEM method seems promising in an idealised problem, its application in a realistic model might present some difficulties:

- As they depend on the velocity, the extended shape functions vary in time. They thus need to be updated after each temporal iteration. The solution at time $t + \Delta t$ is expressed as a linear combination of the shape functions defined at time t . However the test functions at time $t + \Delta t$ must be used to compute the next time step. It is thus necessary to use two different sets of shape/test functions.
- The shape functions are expressed as a function of the normal distance from the boundary. This distance can be complex to define in a realistic two-dimensional domain.
- The enrichment is performed only near the boundary, which can be difficult to handle in a general finite elements code.
- The steepness of the enriched shape functions requires a very high order integration rule. While an exact integration can be performed in the one-dimensional model, it can be more complex in a two-dimensional framework. A possible solution would be to develop integration rules specifically designed for the function to integrate, but this is not straightforward.

D Influence of the boundary condition on the oscillations

Starting from the non-dimensional finite-difference discretisation of the residence time (30), the parameterisation of the boundary layer (10) is now applied to the inflow boundary, while a Dirichlet boundary condition is still used at the outflow boundary:

$$\begin{aligned} \frac{\tilde{\theta}_1^h - \tilde{\theta}_0^h}{\Delta \tilde{x}} &= \frac{e^{-Pe \frac{L^*}{L}}}{1 - e^{-Pe \frac{L^*}{L}}} Pe \left(\frac{\tilde{\theta}_1^h + \tilde{\theta}_0^h}{2} + \frac{L^*}{L} \right) - 1, \\ \frac{\tilde{\theta}_N^h + \tilde{\theta}_{N+1}^h}{2} &= 0. \end{aligned} \quad (40)$$

The solution of the discrete problem is still of the form (32). However, due to the different boundary conditions, the coefficients modify to:

$$A = \frac{2Pe(1 + \frac{L^*}{L})}{Pe(1+r)(r^N - 1) + 2N(e^{\frac{L^*}{L}Pe} - 1)(r-1)}, \quad (41)$$

$$B = -\frac{1}{N}, \quad (42)$$

$$C = \frac{2N(e^{\frac{L^*}{L}Pe} - 1)(r-1)(1+2N) - Pe(1+r) \left[1 + 2N + r^T(2\frac{L^*}{L}N - 1) \right]}{2N \left[Pe(1+r)(r^N - 1) + 2N(e^{\frac{L^*}{L}Pe} - 1)(r-1) \right]}. \quad (43)$$

When the mesh Peclet number $Pe\Delta\tilde{x}$ is higher than 2, the oscillating mode is still present. The amplitude of the oscillations is controlled by the constant A . Figure 10 shows that if we use a Dirichlet inflow boundary condition, the norm of this constant will increase with the mesh Peclet number. If the mesh Peclet number is high, the solution will inevitably show significant oscillations. If the parameterisation of the inflow boundary layer is used with a sufficiently large $\frac{L^*}{L}$, the oscillatory part of the solution is limited and decreases as the mesh Peclet number increases (Figure 10). This is due to the fact that, for a high mesh Peclet number, the boundary layer is entirely comprised in the parameterised zone. The parameterisation used with $\frac{L^*}{L} = 0$ produces the same results as the Dirichlet boundary condition. It is then necessary to use a sufficiently large value of $\frac{L^*}{L}$ to limit the oscillating part of the solution.

Fig. 1 Residence time for the dimensionless, steady-state one-dimensional problem for various Peclet numbers. The thick curve represents the analytical solution. The thin curve represents the numerical solution obtained with a classical finite element method where the circles indicate the mesh nodes. The dimensionless thickness of the boundary layer is Pe^{-1} . The mesh Peclet number is defined by $Pe^h = U\Delta x/K$, where Δx is the grid spacing.

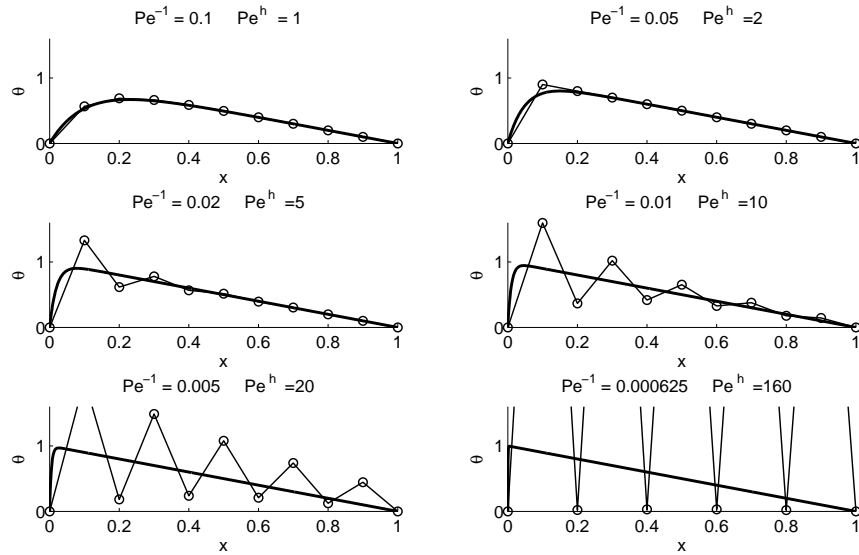


Fig. 2 Residence time for the dimensionless, steady-state one-dimensional problem for various Peclet numbers (the label on the curves indicates the mesh Peclet number, which is $0.1Pe$ in this case). The simulation configuration corresponds to Figure 1. Dashed vertical lines correspond to the mesh nodes position. (a) Analytical solution, (b) Boundary layer treated using the X-FEM method, (c) Parameterised boundary layer.

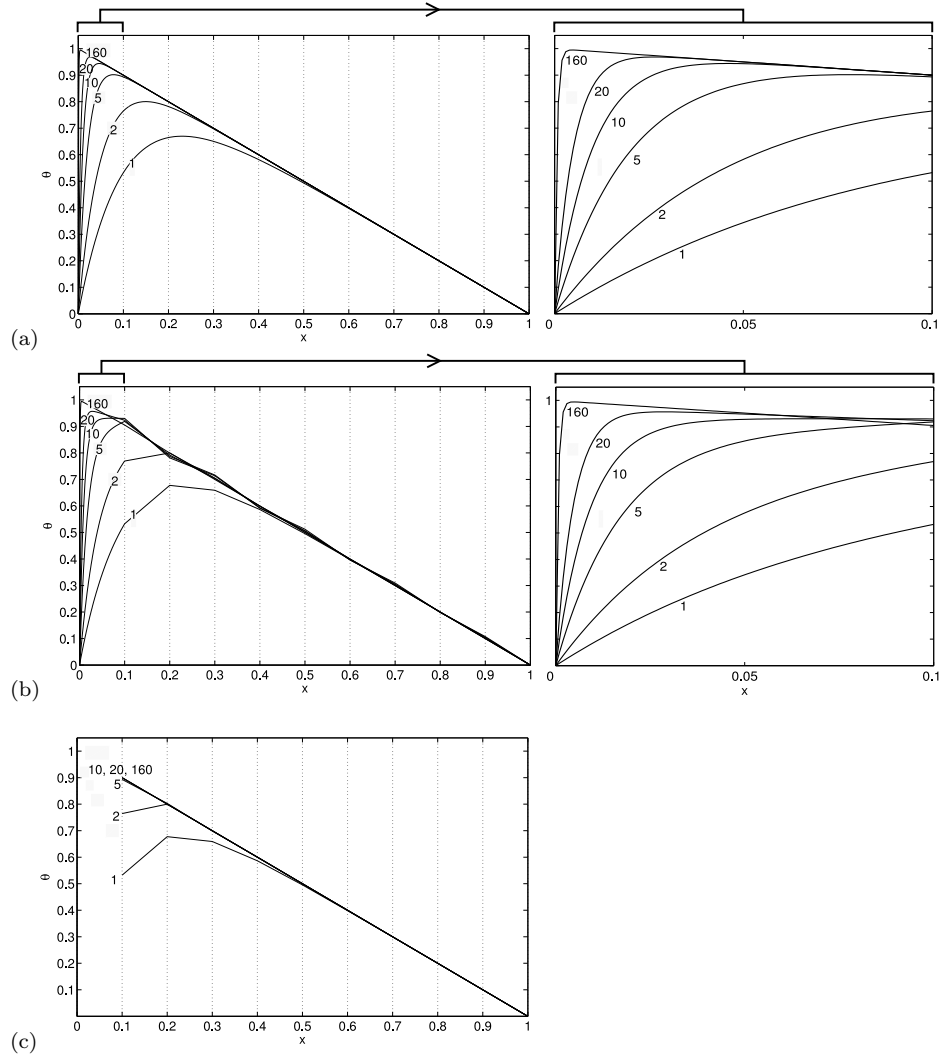


Fig. 3 Parameterisation of the boundary layer for the residence time. The numerical domain boundary is moved to avoid the computation of the boundary layer.

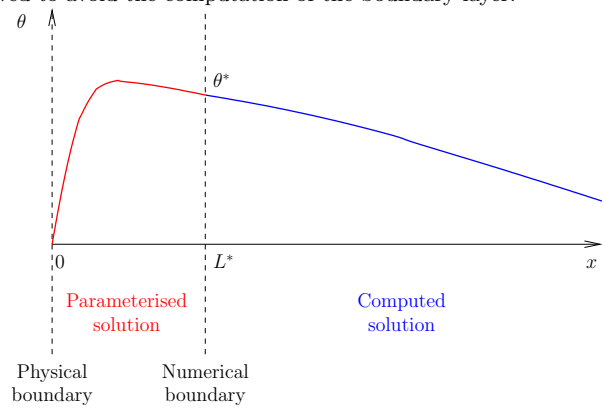


Fig. 4 Evolution of the residence time for the transient one-dimensional problem, after an initialisation of 30 tidal periods ($\tau' = \frac{\tau}{T_{\text{tide}}} - 30$). The colorbar indicates the residence time. (a) High-resolution solution, (b) Boundary layer treated using the X-FEM method, (c) Parameterised boundary layer.

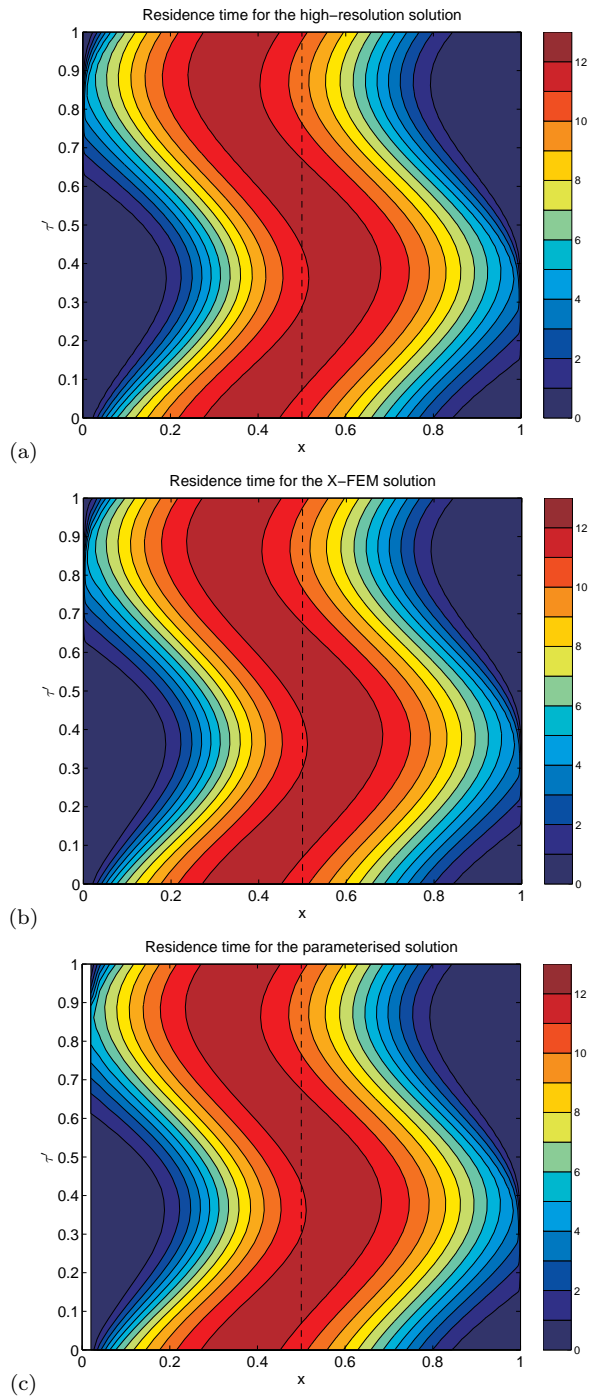


Fig. 5 Unstructured mesh used for the numerical simulations, with a zoom on the Scheldt Estuary (lower panel). The blue part of the mesh (Scheldt Estuary) is used for the residence time computations. The mesh is made up of 26000 triangular elements, and 5000 among them are located in the Scheldt Estuary. The river and its tributaries are represented by 350 one-dimensional elements. The mesh resolution is about 400 *m* in the one-dimensional rivers and varies from 150 metres to 30 kilometres in the two-dimensional domain.

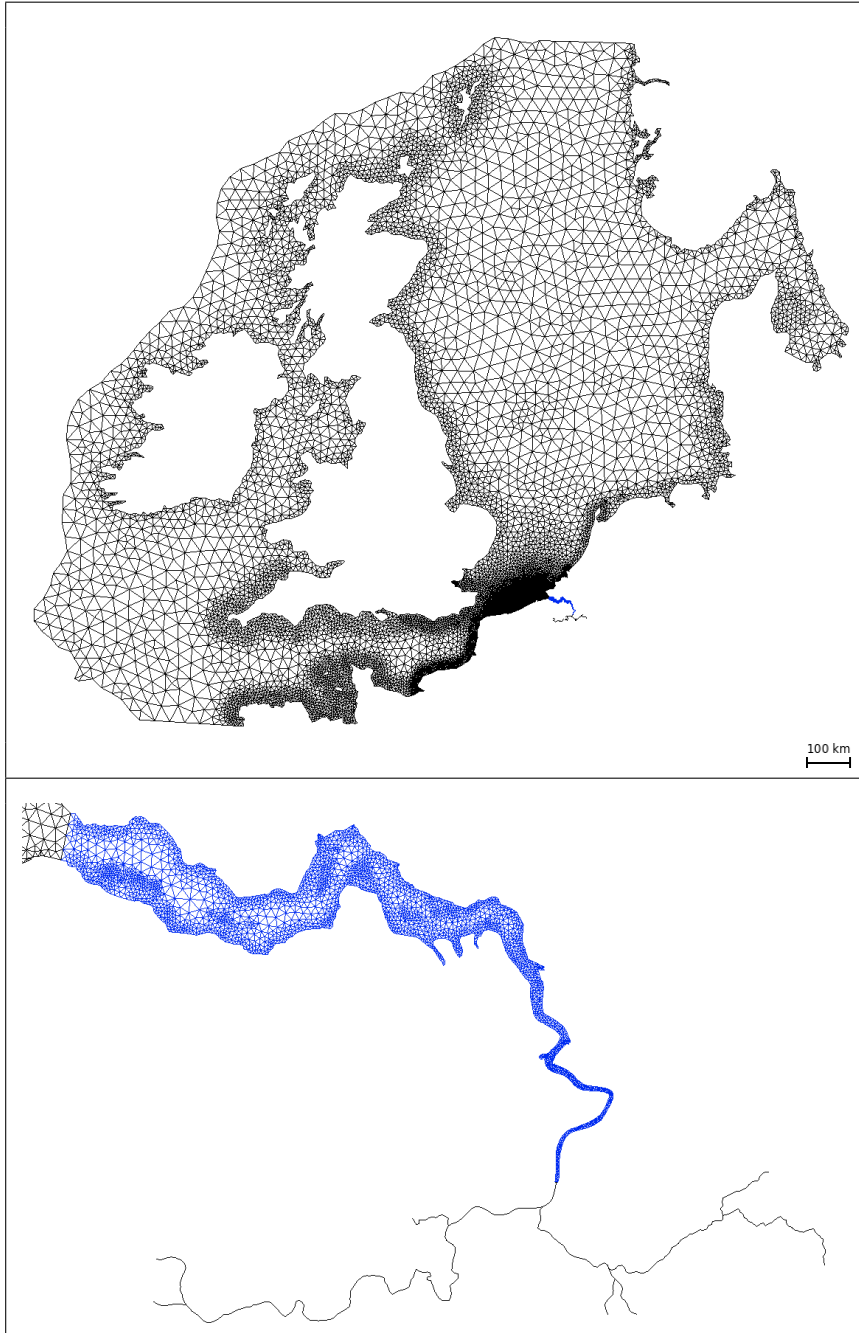
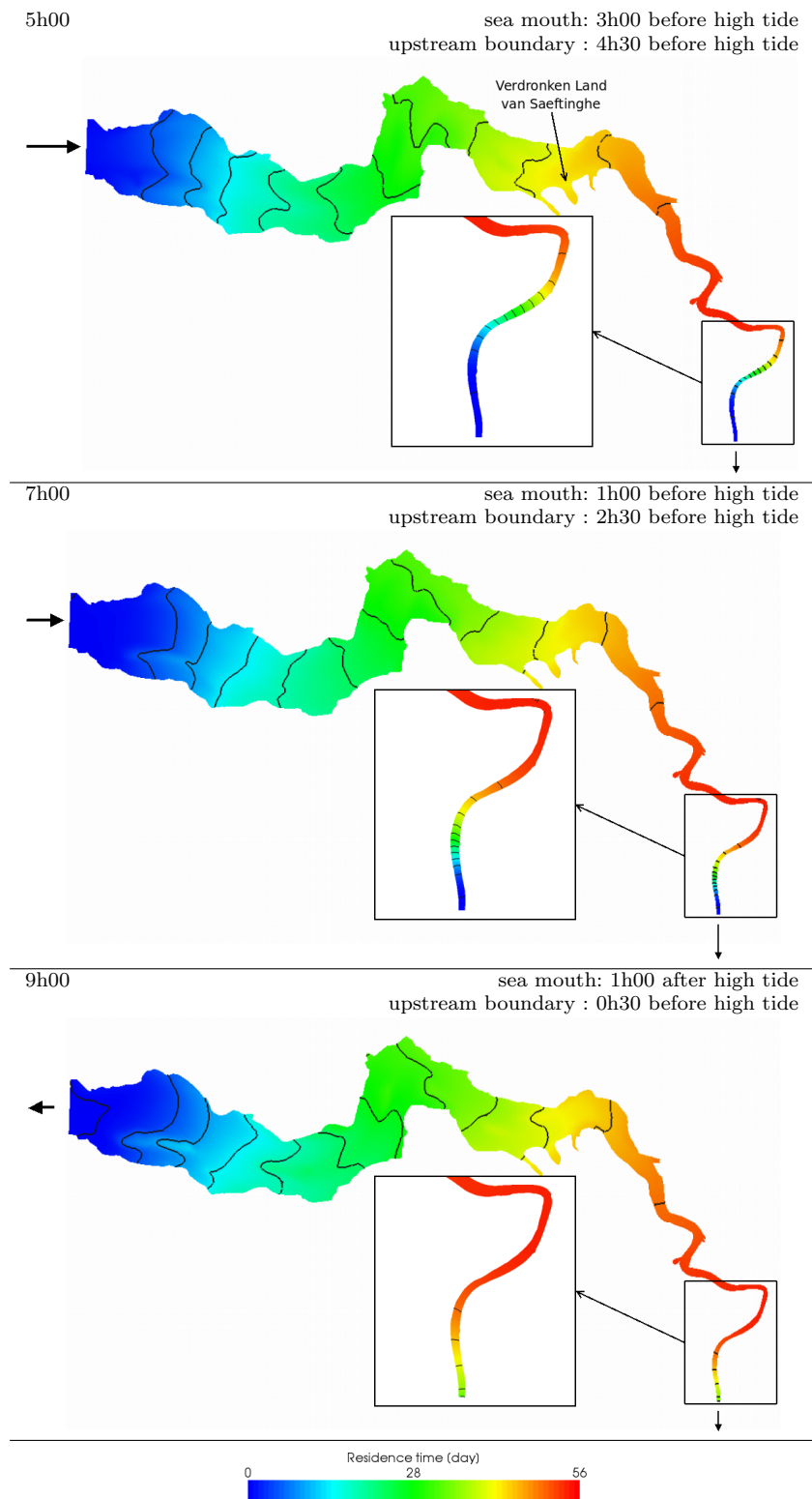
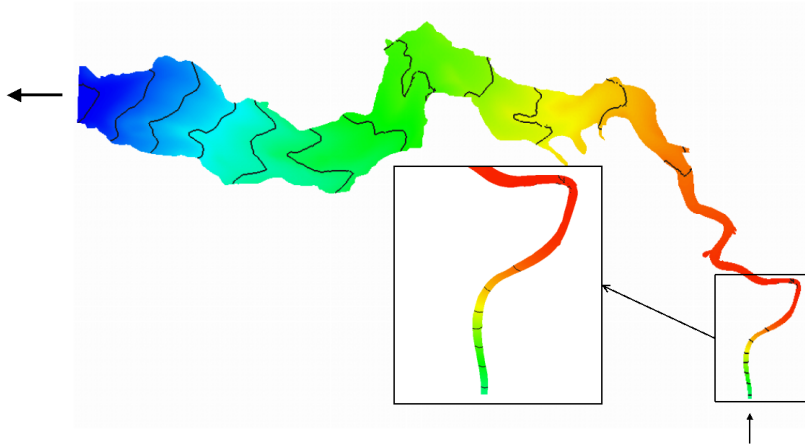


Fig. 6 Residence time in the Scheldt Estuary on February 1, 2001 during a tidal period. The arrows are a qualitative indication of the transport through open boundaries. The residence time interval between isolines is five days.



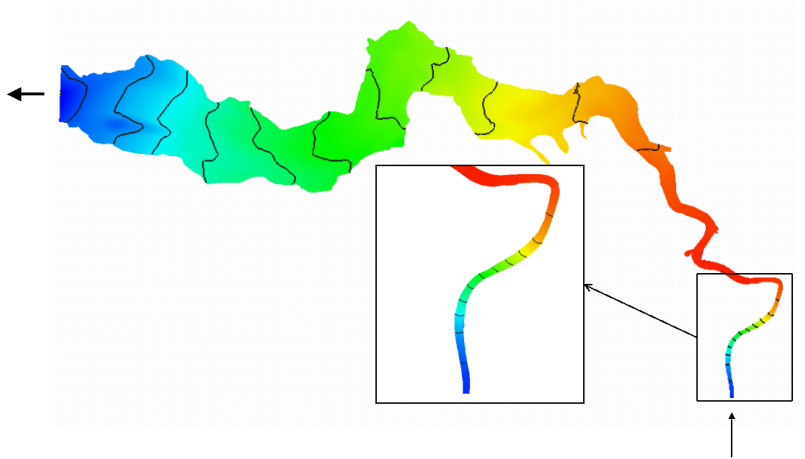
11h00

sea mouth: 3h00 after high tide
upstream boundary : 1h30 after high tide



13h00

sea mouth: 1h15 before low tide
upstream boundary : 2h45 before low tide



15h00

sea mouth: 0h45 after low tide
upstream boundary : 0h45 before low tide

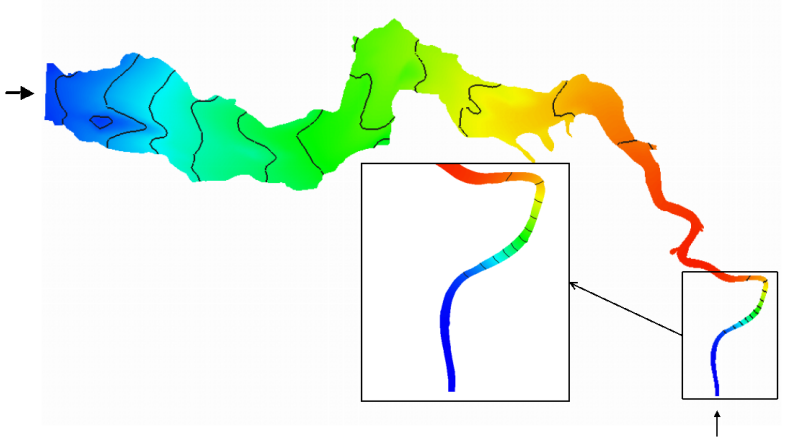


Fig. 7 Mean residence time over the estuarine domain. The red curve represents a one day running mean taken to filter out tidal oscillation. Results between the dashed line (November 1, 2001) and December 31, 2001 correspond to the initialisation of the backward simulation and cannot be trusted (a period of twice the order of magnitude of the residence time, following Delhez et al. (2004b)).

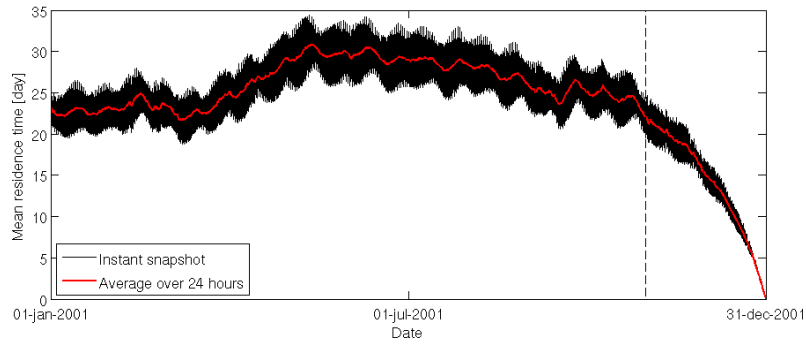


Fig. 8 Amplitude of the residence time variations associated with the M_2 , S_2 and M_{SF} tidal components, in days.

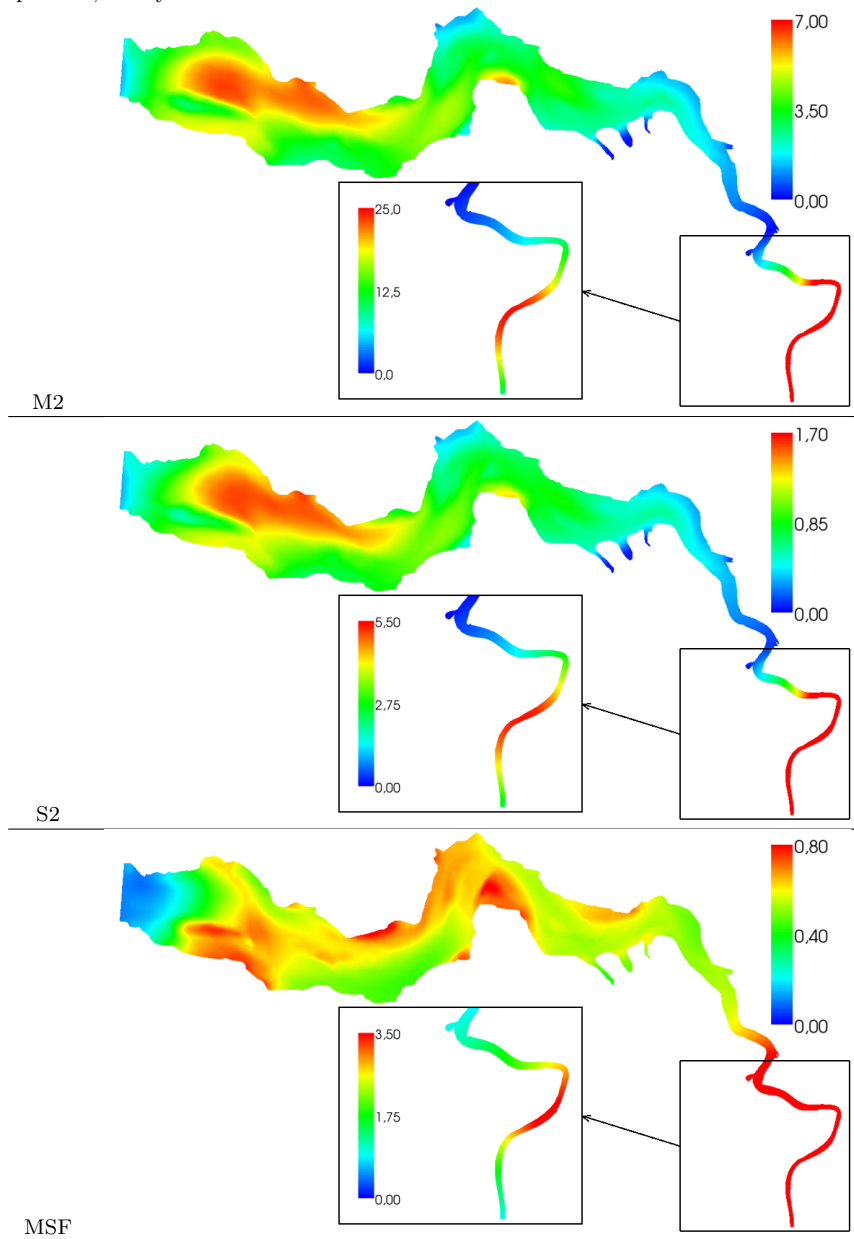


Fig. 9 Residence time along the line A-B on February 1, 2001 during a tidal period. Solutions using the parameterisation of the boundary layer (black) and a Dirichlet boundary condition (red).

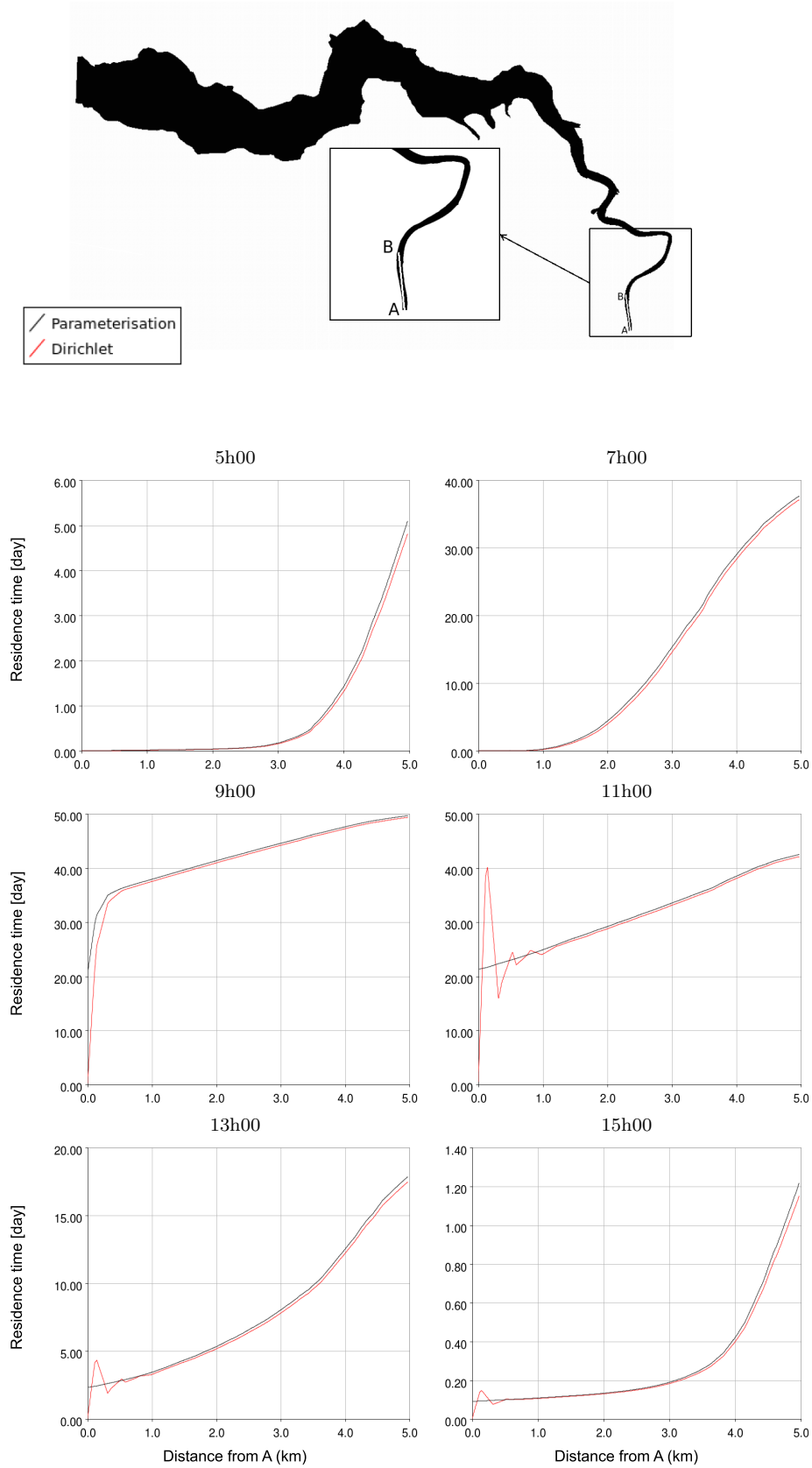
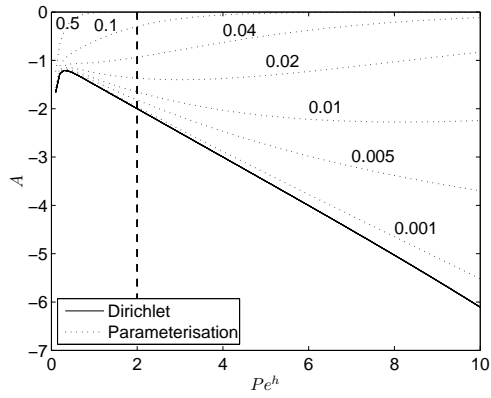


Fig. 10 Evolution of the constant A from equation (32) with the mesh Peclet number $Pe\Delta\bar{x}$ for the stationary one-dimensional problem. Results obtained using a Dirichlet boundary condition (plain line) and the parameterisation of the inflow boundary layer (dotted lines). The values along the curves indicate different parameterised length L^*/L used for the parameterisation of the boundary layer. The dashed line indicates a mesh Peclet number of 2 under which the solution does not present any oscillation. The number of nodes $N = 10$.



References

- Alexe, M., Sandu, A., 2009. Forward and adjoint sensitivity analysis with continuous explicit runge-kutta schemes. *Applied Mathematics and Computation* 208 (2), 328 – 346.
- Allen, C. M., May 1982. Numerical Simulation of Contaminant Dispersion in Estuary Flows. Royal Society of London Proceedings Series A 381, 179–194.
- Arega, F., Armstrong, S., Badr, A., 2008. Modeling of residence time in the East Scott Creek Estuary, South Carolina, USA. *Journal of Hydro-environment Research* 2 (2), 99 – 108.
- Arminjon, P., Dervieux, A., 1993. Construction of TVD-like artificial viscosities on two-dimensional arbitrary FEM grids. *Journal of Computational Physics* 106 (1), 176 – 198.
- Black, K. P., Gay, S. L., 1987. Eddy formation in unsteady flows. *Journal of Geophysical Research* 92 (C9), 9514–9522.
- Blumberg, A. F., Mellor, G. L., 1987. A description of three-dimensional coastal ocean circulation model. In: Heaps, N. S. (Ed.), *Three Dimensional Coastal Ocean Model*. American Geophysical Union, pp. 1–16.
- Bolin, B., Rhode, H., 1973. A note on the concepts of age distribution and residence time in natural reservoirs. *Tellus* 25, 58–62.
- Burchard, H., 2002. Applied Turbulence Modelling in Marine Waters. No. 100 in *Lecture Notes in Earth Science*. Springer.
- Cockburn, B., Shu, C.-W., 1998. The Runge-Kutta discontinuous Galerkin method for conservation laws V - multidimensional systems. *Journal of Computational Physics* 141, 191–224.
- Combescuré, A., Gravouil, A., Baïetto-Dubourg, M.-C., Elguedj, E., Ribeaucourt, R., Ferri, E., 2005. Extended finite element method for numerical simulation of 3d fatigue crack growth. In: D. Dowson, M. Priest, G. D., Lubrecht, A. (Eds.), *Life Cycle Tribology - Proceedings of the 31st Leeds-Lyon Symposium on Tribology Held at Trinity and All Saints College, Horsforth, Leeds, UK 7th–10th September 2004*. Vol. 48 of *Tribology and Interface Engineering Series*. Elsevier, pp. 323 – 328.
- Comblen, R., Lambrechts, J., Remacle, J.-F., Legat, V., 2009. Practical evaluation of five part-discontinuous finite element pairs for the non-conservative shallow water equations. *International Journal for Numerical Methods in Fluids*, doi:10.1002/flid.2094.
- de Brye, B., de Brauwere, A., Gourgue, O., Kärna, T., Lambrechts, J., Comblen, R., Deleersnijder, E., 2009. A Finite-Element, Multi-Scale Model of the Scheldt Tributaries, River, Estuary and ROFI. *Coastal Engineering*, under revision.
- Deleersnijder, E., 1993. Numerical mass conservation in a free-surface sigma coordinate marine model with mode splitting. *Journal of Marine Systems* 4, 365–370.
- Deleersnijder, E., Campin, J.-M., Delhez, E. J. M., 2001. The concept of age in marine modelling: I. theory and preliminary model results. *Journal of Marine Systems* 28 (3-4), 229 – 267.
- Deleersnijder, E., Delhez, E. J. (Eds.), 2007. Timescale- and tracer-based methods for understanding the results of complex marine models. Vol. 74, 585-776 (Special issue). *Estuarine, Coastal and Shelf Science*.
- Delhez, E. J., Lacroix, G., Deleersnijder, E., 2004a. The age as a diagnostic of the dynamics of marine ecosystem models. *Ocean Dynamics* 54 (2), 221 – 231.
- Delhez, E. J. M., 2006. Transient residence and exposure times. *Ocean Science* 2 (1), 1–9.
- Delhez, E. J. M., Deleersnijder, E., 2006. The boundary layer of the residence time. *Ocean Dynamics* 56, 139–150.
- Delhez, E. J. M., Heemink, A. W., Deleersnijder, E., 2004b. Residence time in a semi-enclosed domain from the solution of an adjoint problem. *Estuarine, Coastal and Shelf Science* 61, 691–702.
- Egbert, G. D., Bennett, A. F., Foreman, M. G. G., 1994. TOPEX/POSEIDON tides estimated using a global inverse model. *Journal of Geophysical Research* 99, 24,821–24,852.
- Elden, L., 1982. Time Discretization in the Backward Solution of Parabolic Equations. II. *Mathematics of Computation* 39 (159), 69–84.
- Garabedian, P. R., 1964. *Partial Differential Equations*. John Wiley & Sons, Inc., New York.
- Gourgue, O., Deleersnijder, E., White, L., 2007. Toward a generic method for studying water renewal, with application to the epilimnion of Lake Tanganyika. *Estuarine, Coastal and Shelf Science* 74, 764–776.
- Hanert, E., Deleersnijder, E., Blaise, S., Remacle, J.-F., 2007. Capturing the bottom boundary layer in finite element ocean models. *Ocean Modelling* 17, 153–162.

- Kalnay, E., Kanamitsu, M., Kistler, R., Collins, W., Deaven, D., Gandin, L., Iredell, M., Saha, S., White, G., Woollen, J., Zhu, Y., Leetmaa, A., Reynolds, B., Chelliah, M., Ebisuzaki, W., Higgins, W., Janowiak, J., Mo, K. C., Ropelewski, C., Wang, J., Jenne, R., Joseph, D., 1996. The NCEP/NCAR 40-Year Reanalysis Project. *Bulletin of the American Meteorological Society* 77, 437–472.
- Kuzmin, D., Löhner, R., Turek, S. (Eds.), 2005. Flux-Corrected Transport. Principles, Algorithms and Applications. Springer.
- Liu, C.-S., Chang, C.-W., Chang, J.-R., 2008a. The backward group preserving scheme for 1d backward in time advection-dispersion equation. *Numerical Methods for Partial Differential Equations* 26 (1), 61–80.
- Liu, W.-C., Chen, W.-B., Kuo, J.-T., Wu, C., 2008b. Numerical determination of residence time and age in a partially mixed estuary using three-dimensional hydrodynamic model. *Continental Shelf Research* 28 (8), 1068 – 1088.
- Luther, K. H., Haitjema, H. M., 1998. Numerical experiments on the residence time distributions of heterogeneous groundwatersheds. *Journal of Hydrology* 207 (1-2), 1 – 17.
- Meyers, S. D., Luther, M. E., 2008. A numerical simulation of residual circulation in Tampa Bay. part II: Lagrangian residence time. *Estuaries and Coasts* 31, 815–827.
- Moës, N., Dolbow, J., Belytschko, T., 1999. A finite element method for crack growth without remeshing. *International Journal for Numerical Methods in Engineering* 46, 131–150.
- Monsen, N. E., Cloern, J. E., Lucas, L. V., Monismith, S. G., 2002. A comment on the use of flushing time, residence time, and age as transport time scales. *Limnology and oceanography* 47, 1545–1553.
- Nauman, E. B., 1981. Residence time distributions in systems governed by the dispersion equation. *Chemical Engineering Science* 36 (6), 957 – 966.
- Pawlowicz, R., Beardsley, B., Lentz, S., 2002. Classical tidal harmonic analysis including error estimates in MATLAB using T_TIDE. *Computers and Geosciences* 28, 929–937.
- Payne, L. E., 1975. Improperly Posed Problems in Partial Differential Equations. Regional Conference Series in Applied Mathematics. Society for Industrial and Applied Mathematics.
- Soetaert, K., Herman, P. M. J., 1995. Estimating estuarine residence times in the Westerschelde (The Netherlands) using a box model with fixed dispersion coefficients. *Hydrobiologia* 311, 215–224.
- Spivakovskaya, D., Hemink, A. W., Deleersnijder, E., 2007. Lagrangian modelling of multi-dimensional advection-diffusion with space-varying diffusivities: theory and idealized test cases. *Ocean Dynamics* 57, 189 – 203.
- Steen, R. J. C. A., Evers, E. H. G., Hattum, B. V., Cofino, W. P., Brinkman, T. U. A., 2002. Net fluxes of pesticides from the Scheldt Estuary into the North Sea: a model approach. *Environmental Pollution* 116 (1), 75 – 84.
- Takeoka, H., 1984. Fundamental concepts of exchange and transport time scales in a coastal sea. *Continental Shelf Research* 3 (3), 311 – 326.
- Tartinville, B., Deleersnijder, E., Rancher, J., 1997. The water residence time in the Mururoa atoll lagoon: sensitivity analysis of a three-dimensional model. *Coral Reefs* 16, 193–203.
- Thuburn, J., Haine, T. W. N., 2001. Adjoints of nonoscillatory advection schemes. *Journal of Computational Physics* 171, 616 – 631.
- Wang, C.-F., Hsu, M.-H., Kuo, A. Y., 2004. Residence time of the Danshuei River estuary, Taiwan. *Estuarine, Coastal and Shelf Science* 60 (3), 381 – 393.
- White, L., Legat, V., Deleersnijder, E., 2008. Tracer Conservation for Three-Dimensional, Finite-Element, Free-Surface, Ocean Modeling on Moving Prismatic Meshes. *Monthly Weather Review* 136, 420–442.
- Wyart, E., DufLOT, M., Coulon, D., Martiny, P., Pardoën, T., Remacle, J.-F., Lani, F., 2008. Substructuring FE-XFE approaches applied to three-dimensional crack propagation. *Journal of Computational and Applied Mathematics* 215 (2), 626 – 638.
- Zimmerman, J. T. F., 1976. Mixing and flushing of tidal embayments in the western dutch Wadden Sea. Part I: distribution of salinity and calculation of mixing time scales. *Netherlands Journal of Sea Research* 10, 149–191.